

## Compositional analysis by RBS, XPS and EDX of ZnO:Al,Bi and ZnO:Ga,Bi thin films deposited by d.c. magnetron sputtering

J.M. Ribeiro<sup>a</sup>, F.C. Correia<sup>a</sup>, P.B. Salvador<sup>a</sup>, L. Rebouta<sup>a</sup>, L.C. Alves<sup>b</sup>, E. Alves<sup>b</sup>, N.P. Barradas<sup>b,c</sup>, A. Mendes<sup>d</sup>, C.J. Tavares<sup>a,\*</sup>

<sup>a</sup> Centre of Physics, University of Minho, 4804-533, Guimarães, Portugal

<sup>b</sup> Institute for Plasmas and Nuclear Fusion, IST, University of Lisbon, Lisbon, Portugal

<sup>c</sup> Centre for Nuclear Sciences and Technologies, IST, University of Lisbon, Bobadela, Portugal

<sup>d</sup> LEPABE, Faculty of Engineering of the University of Porto, Rua Roberto Frias s/n, 4200-465, Porto, Portugal

### ARTICLE INFO

#### Keywords:

ZnO  
Bismuth  
RBS  
XPS  
Thermoelectric  
TCO  
PIXE  
Al  
Ga  
Doping

### ABSTRACT

Rutherford backscattering spectrometry, X-ray photoelectron and X-ray energy dispersive spectroscopies were employed to analyse Bi incorporation into ZnO:Al and ZnO:Ga transparent and electrically conductive thin films deposited by d.c. magnetron sputtering, with thickness in the range of 300–400 nm. Sputtering was performed in an argon atmosphere from two targets in confocal geometry being one composed of either ZnO:Al<sub>2</sub>O<sub>3</sub> or ZnO:Ga<sub>2</sub>O<sub>3</sub> composites and the other a Bi metal target. The content of bismuth dopant in the ZnO matrix was controlled by the respective target current density ( $J_{\text{Bi}}$ ) in order to attain a high optical transparency (> 80%) in the visible region. For ZnO:Al,Bi films Bi content varied from 0.1 to a maximum of 1.5 at.% when varying  $J_{\text{Bi}}$  from 0.06 to 0.26 mA cm<sup>-2</sup>. However, for ZnO:Ga,Bi films, deposited in similar conditions, Bi reached a maximum overall layer content of 2.4 at.%, with a surface enrichment content that varied from 1.3 to 8.8 at.%. It was also observed that the Bi content in the topmost layers of the films is slightly depleted due to thermal evaporation upon thermal annealing in vacuum at 350 °C. It is envisaged applications for these films as transparent photoelectrodes and thermoelectric materials.

### 1. Introduction

Zinc oxide is a semiconductor with interesting physical-chemical properties that have drawn consideration to several fields of research and applications. In particular, as a transparent conductive oxide (TCO) has a direct band-gap of ~3.4 eV at room temperature, which grants optoelectronic applicability in the near-UV range, such as in photo-detectors, light-emitting diodes, photovoltaics, gas sensing and thin-film transistors [1–6], to name a few. ZnO versatility concerning the deposition technique is very attractive. Pulsed laser deposition (PLD), molecular beam epitaxy (MBE), atomic layer deposition (ALD), chemical synthesis and magnetron sputtering have been extensively applied in the research community [7–10]. The ZnO compound crystallizes in the hexagonal wurtzite structure and displays an intrinsic n-type conductivity that can be further enhanced to lower the electrical resistivity for the use in optoelectronic devices. By doping ZnO with Group IIIB elements, such as Ga and Al, n-type carrier concentration and electrical conductivity can be increased by more than 3–4 orders of magnitude [11–13]. Furthermore, besides the fact that doped ZnO films

are prominent candidates for applications as TCOs, some authors have reported interesting thermoelectric properties as well [14–16]. In this work, ZnO:Ga,Bi and ZnO:Al,Bi thin films were produced by magnetron sputtering in confocal geometry with the aim to produce high quality thermoelectric cells, with high optical transparency and a power factor that envisages these materials for industrial applications. Since Bi<sup>3+</sup> is a heavier ion with a very large ionic radius (1.03 Å), in comparison to that of Zn<sup>2+</sup> (0.60 Å), it is expected that when the former substitutes the latter in the ZnO wurtzite structure it will hinder phonon vibrations throughout the lattice, hence contributing to the decrease of the thermal conductivity and subsequently enhancing the thermoelectric figure of merit and, indirectly, the thermoelectric power, as reported elsewhere by the authors [16]. Composition information on ZnO:Ga,Bi and ZnO:Al,Bi thin films is scarce or non-existent in the literature. Hence, an in-depth study on the Bi dopant concentration on these films was endured by the authors, using highly-sensitive characterization techniques such as Rutherford backscattering spectrometry (RBS), Particle-induced X-ray emission (PIXE), X-ray photoelectron spectroscopy (XPS) and Energy dispersive X-ray spectroscopy (EDX).

\* Corresponding author.

E-mail address: [ctavares@fisica.uminho.pt](mailto:ctavares@fisica.uminho.pt) (C.J. Tavares).

<https://doi.org/10.1016/j.vacuum.2018.12.038>

Received 25 October 2018; Received in revised form 11 December 2018; Accepted 22 December 2018

Available online 24 December 2018

0042-207X/© 2019 Elsevier Ltd. All rights reserved.

## 2. Experimental details

In order to dope the ZnO with Bi, Ga and Al, confocal geometry was used with two circular magnetrons (10 cm diameter) in a home-made d.c. magnetron sputtering system (Fig. 1). A 99.95% purity bismuth target was used for Bi doping (FHR Anlagenbau GmbH) and two intrinsically doped ZnO targets were used for the ZnO:Ga (GZO) and ZnO:Al (AZO) matrixes (ZnO(95.5)Ga<sub>2</sub>O<sub>3</sub>(4.5) wt.% target, 99.95% purity; ZnO(98)Al<sub>2</sub>O<sub>3</sub>(2) wt.%, 99.95% purity; FHR Anlagenbau GmbH); respectively. ZnO:Ga,Bi and ZnO:Al,Bi thin films were deposited on Si substrates (SIEGERT WAFER GmbH, Part-No: L14016) with <100> orientation. All substrates were previously cleaned with isopropanol in an ultrasound bath for 15 min. Prior to deposition, the substrates were etched in an Ar<sup>+</sup> plasma at 2 Pa to further clean the exposed surfaces. The samples were fixed to a sample holder in the middle of the chamber with Kapton tape, radially symmetrical to the centre of the sample holder, fixed at 9 cm (vertically) from the normal to the centre of the targets, in a spinning platform to assure a homogeneous deposition. Several parameters were kept constant throughout all depositions, such as deposition time (20 min), current density on the intrinsically doped targets (5.0 mA cm<sup>-2</sup>), substrate rotation speed (18 r.p.m), deposition temperature (200 °C), argon flow (40 sccm), which corresponds to a working pressure of 0.37 Pa, and a substrate bias of -60 V. The vacuum deposition chamber was baked with external sleeves for an hour prior to the deposition, in order to reduce the base pressure for each deposition (~10<sup>-4</sup> Pa). The current density applied to the Bi target, J<sub>Bi</sub>, was varied throughout the series of samples from 0 to 0.26 mA cm<sup>-2</sup>. Post-deposition three-staged thermal treatments were performed at 350 °C for ZnO:Al,Bi and ZnO:Ga,Bi films; these consisted in a 90 min ramp to the desired temperature, followed by a 120 min stage and cooling to room temperature, corresponding to approximately 6 h for all thermal treatments. The thicknesses of all films are in the range of 300–400 nm.

Rutherford backscattering spectrometry and Particle-induced X-ray emission measurements were performed at the Laboratory of Accelerators and Radiation Technologies of Instituto Superior Técnico (Lisbon), using a Van de Graaff accelerator. In this measurement, a small chamber was used where three detectors are installed: standard at 140°, and two pin-diode detectors located symmetrical to each other, both at 165°. Spectra were collected for 2.0 MeV <sup>4</sup>He<sup>+</sup>. Normal incidence was used in the experiments. The RBS data were analysed with the NDF code [17]. X-ray photoelectron spectroscopy experiments were carried out using monochromatic Al-K<sub>α</sub> radiation (1486.6 eV) from a Kratos Axis-Supra instrument, from 3Bs Group, University of Minho. Photoelectrons were collected from a take-off angle of 90° relative to the sample surface. The measurement was done in a Constant Analyser Energy mode (CAE) with a

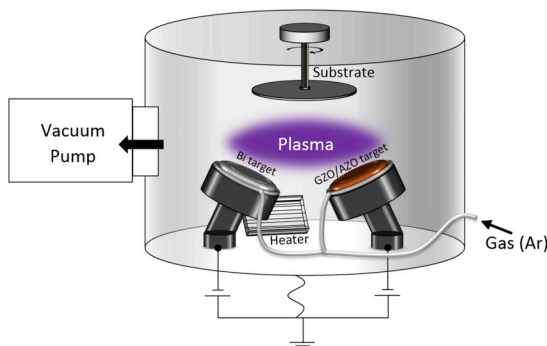


Fig. 1. Custom confocal sputtering system used for the deposition of ZnO:Al,Bi and ZnO:Ga,Bi films.

160 eV pass energy and 15 mA of emission current for survey spectra and 40 eV pass energy for high resolution spectra, using an emission current of 15 mA. Charge referencing was done by setting the lower binding energy of the C1s hydrocarbon peak at 248.8 eV; an electron flood gun was used to minimize surface charging. Energy-dispersive X-ray spectroscopy was performed with an equipment from EDAX incorporated in a FEI NOVA NanoSEM 200 scanning electron microscope, at SEMAT/UM, University of Minho. X-ray diffraction (XRD) grazing incidence (1.5°) experiments were carried out using Cu K<sub>α</sub> radiation in a Bruker AXS D8 diffractometer, at SEMAT/UM, University of Minho.

## 3. Results and discussion

### 3.1. ZnO:Al,Bi films

Fig. 2 contains information on the dopant Bi content in ZnO:Al,Bi films as function of the Bi target current density, J<sub>Bi</sub>, measured by different analytical techniques. In this figure, blue symbols represent as-deposited (AD) samples, while red ones represent samples after a thermal annealing in vacuum at 350 °C (TA). Note that the RBS measurements were performed in-depth analyzing the whole film thickness (~300 nm), and the presented data is an average from this. Starting with the EDX data, it can be observed an exponential tendency in the increase of the Bi content with J<sub>Bi</sub>, as expected. The Bi content starts at 0.1 at.% for J<sub>Bi</sub> = 0.06 mA cm<sup>-2</sup>, passes through an average of 0.6 at.% for J<sub>Bi</sub> of 0.19 mA cm<sup>-2</sup> and finally reaches a maximum with an average of 1.3 at.% for J<sub>Bi</sub> = 0.26 mA cm<sup>-2</sup>. Both RBS and XPS data confirm this tendency in Bi content, as represented in Fig. 2. With RBS, values of 0.1 at.% of Bi in ZnO:Al,Bi films were obtained for samples deposited with J<sub>Bi</sub> = 0.13 mA cm<sup>-2</sup> and ~0.7 at.% for both as-deposited and thermal annealed (in vacuum at 350 °C) films deposited with J<sub>Bi</sub> = 0.22 mA cm<sup>-2</sup>. With XPS, one measurement was taken for J<sub>Bi</sub> = 0.26 mA cm<sup>-2</sup> and the corresponding Bi content stands for 1.0 at.%. Error bars for Bi atomic composition are represented in this figure, being an average of 3% for RBS values and an average of 5% for XPS and EDX findings.

From Fig. 2 it can be seen a slight decrease in Bi content was registered in some thermal annealed samples, when compared to as-deposited, possibly due to Bi diffusion to the surface, resulting in a lower concentration in the bulk. Moreover, when comparing Bi

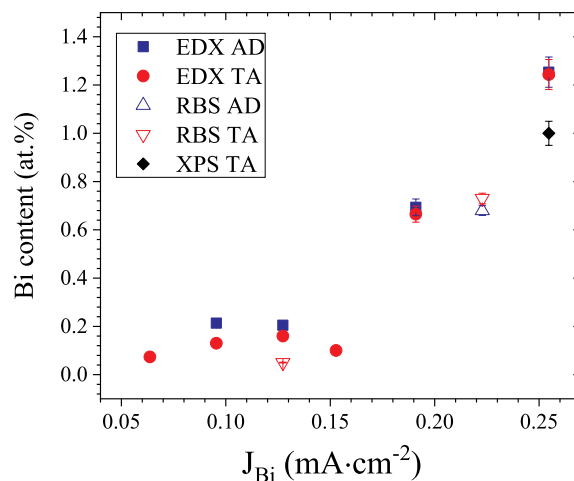


Fig. 2. Bi at. % content of ZnO:Al,Bi thin films as function of Bi target current density, J<sub>Bi</sub>, from EDX, RBS and XPS analyses. Data is represented for as-deposited (AD) and thermal annealed in vacuum at 350 °C (TA) films.

content for  $J_{\text{Bi}} = 0.26 \text{ mA cm}^{-2}$  it can be observed that the EDX data registers a maximum of 1.3 at.% (for both AD and TA samples), whereas from XPS analysis on the same TA sample registers a value slightly lower of 1.0 at.% is registered. The melting temperature of Bi is lower ( $\sim 271 \text{ }^\circ\text{C}$ ; at ambient temperature and pressure) than that of the thermal annealing ( $350 \text{ }^\circ\text{C}$ ) in vacuum, hence some of the Bi content at the surface evaporated during this treatment. Nevertheless, the results obtained from different characterization techniques show a good agreement, even taking into account that different film thicknesses were probed: for RBS and EDX,  $\sim 300 \text{ nm}$ ; for XPS 5–7 nm below the sample surface. This means that, for the ZnO:Al:Bi films, the analysed Bi concentration near the surface is similar to the Bi concentration across the film deposit. A certain amount of Bi evaporation during sputtering cannot be discarded since the data trends in Fig. 2 deviate from linearity, in particular for lower amounts of Bi doping, albeit the authors perception that most of the Bi content results from sputtering. Previous experiments at lower deposition rates suggests this, as well as the race track wear on the target corroborates this line of thought.

In comparison to the current density applied to the AZO target ( $5.0 \text{ mA cm}^{-2}$ ), very low current densities are required for the Bi target because: first, as previously mentioned, Bi has a very low melting temperature; second, in order to retain the film optical transparency, finite amounts of Bi atoms are incorporated in the ZnO:Al structure. Hence, the slow evolution of Bi content with  $J_{\text{Bi}}$  reveals that the sputtering yield of Bi is initially very low, as is the energy of the Bi adatoms on the growing film front, and after a certain threshold at  $\sim 0.15 \text{ mA cm}^{-2}$  the incorporation of Bi is substantially enhanced. In particular, the Bi cathode target potential was very low ( $\sim 30 \text{ V}$ ) for the smallest  $J_{\text{Bi}} = 0.03 \text{ mA cm}^{-2}$ , increasing around the aforementioned threshold to  $\sim 230 \text{ V}$ , and reaching a plateau at  $\sim 250 \text{ V}$  for the highest  $J_{\text{Bi}} = 0.26 \text{ mA cm}^{-2}$ .

In Fig. 3 is presented the RBS spectra of a ZnO:Al:Bi film deposited with the  $J_{\text{Bi}} = 0.22 \text{ mA cm}^{-2}$  after thermal annealing in vacuum at  $350 \text{ }^\circ\text{C}$ . The concentration profile of the heavier elements can be easily obtained with a good accuracy from the spectrum using the NDF code. For better understanding, the front edges of the elements are indicated in this figure. These edges correspond to scattering from different elements at the sample surface, where the only energy loss is due to momentum transfer to the target atom. Bi is the heaviest element present, and the corresponding signal from layers closer to the surface is clearly observed at high backscattering energies, separated from the other signals. The high energy edge of the

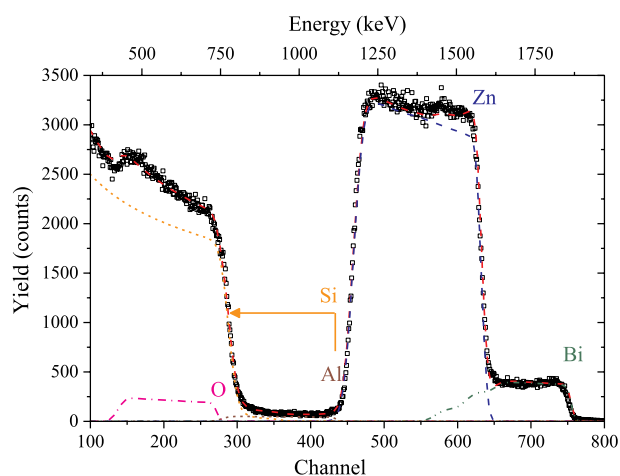


Fig. 3. RBS spectra of a ZnO:Al:Bi thin film deposited with the  $J_{\text{Bi}} = 0.22 \text{ mA cm}^{-2}$  after thermal annealing in vacuum at  $350 \text{ }^\circ\text{C}$ .

Table 1

Average concentration (at.%) of the elements of the host matrix: ZnO:Al.

Element	Zn	O	Al
Concentration (at.%)	$51.2 \pm 1.0$	$44.7 \pm 1.3$	$3.6 \pm 0.4$

bismuth signal near 1.88 MeV corresponds to backscattering from Bi at the surface. The high energy edge of the zinc peak near 1.6 MeV corresponds to backscattering from Zn at the surface and the low energy edge of the Zn peak (about 1.3 MeV) corresponds to scattering from Zn at the film/Si interface. By measuring the energy width of the Zn peak, the thickness of the layer can be calculated. Given that quantification is made from first principles, that is, knowledge of Rutherford scattering cross sections, Bi concentration can be determined with low uncertainty. At deeper layers, Bi signal is superimposed with Zn signal, and the uncertainty in the concentration becomes somewhat larger. Nevertheless, as the entire spectrum is fitted with all elements, included adding to 100 at.%, Bi concentration is rather well defined. In case of the sample shown in Fig. 3, the RBS spectrum indicates a decrease of Bi content near the film/Si substrate interface. However, no significant changes were seen after thermal annealing.

The average concentration of the elements of the host matrix (ZnO:Al) was thus determined from the RBS fits of all samples and is given in Table 1; the Bi dopant concentration is given in Fig. 2. It can be derived from Table 1 that the ZnO:Al:Bi films are deficient in oxygen. This oxygen sub stoichiometry has been already observed by other authors for the case of Al-doped ZnO transparent and electrically conductive thin films, being attributed to the oxygen vacancy generation in the wurtzite cell due to the trivalent  $\text{Al}^{3+}$  dopant [18]. A similar effect was observed in  $\text{TiO}_2\text{:Nb}$  TCO films [19]. The Al content  $3.6 \pm 0.4 \text{ at.}\%$  is considered high when comparing to the composition of the ZnO:Al<sub>2</sub>O<sub>3</sub> sputtering target (1.6 at.%). This resulted in the enhancement of the electrical properties of these thin films, as previously reported [16].

In Fig. 4 is displayed the XPS spectra and respective fits to the main photoelectron lines of the thermal-annealed ZnO:Al:Bi thin film with highest Bi incorporation (1.0 at.%) corresponding to  $J_{\text{Bi}} = 0.26 \text{ mA cm}^{-2}$ . From Fig. 4a) the Zn 2p<sub>3/2</sub> core line was fitted with one component (1021.7 eV; FWHM = 1.7 eV), which is ascribed to Zn–O bonds [20]. Regarding the O 1s core line in Fig. 4b), this was fitted with three components (I, II and III): the main component at 528.1 eV (I) is ascribed with Zn–O bonds; the second component (II) centred at 529.3 eV is associated with defective oxygen (vacancies) and with Bi–O bonds; the third component (III) centred at 530.0 eV is associated with adsorbed oxygen [21,22]. The relative areas of these three contributions is 49%, 31% and 20%, respectively. Component II of the O 1s photoelectron line, related with oxygen vacancies, has a FWHM of 1.2 eV, which reveals the importance of the defective oxygen sites in the enhancement of the electrical conductivity, as reported by the authors elsewhere [16]. In Fig. 4c) the Al 2p<sub>3/2</sub> core line was fitted with one contribution (74.2 eV; FWHM = 1.7 eV) related with either Al–O bonds in the ZnO matrix or with Al<sub>2</sub>O<sub>3</sub> (which cannot be excluded). Lastly, the Bi 4f core level, shown in Fig. 4d), was fitted into peak doublets with a spin-orbit energy separation of  $4f_{5/2}\text{--}4f_{7/2} = 5.3 \text{ eV}$  and a peak ratio  $A_{4f_{5/2}}/A_{4f_{7/2}} = 0.75$ . Two contributions were fitted, with Bi 4f<sub>7/2</sub> binding energies of 156.6 eV (FWHM = 1.4 eV) and 158.9 eV (FWHM = 1.3 eV), which correspond to the metallic bismuth and oxidation state of Bi<sup>3+</sup> in Bi<sub>2</sub>O<sub>3</sub>, respectively [23]. The ratio of this oxide/metal oxidation in this particular sample is  $\sim 3$ .

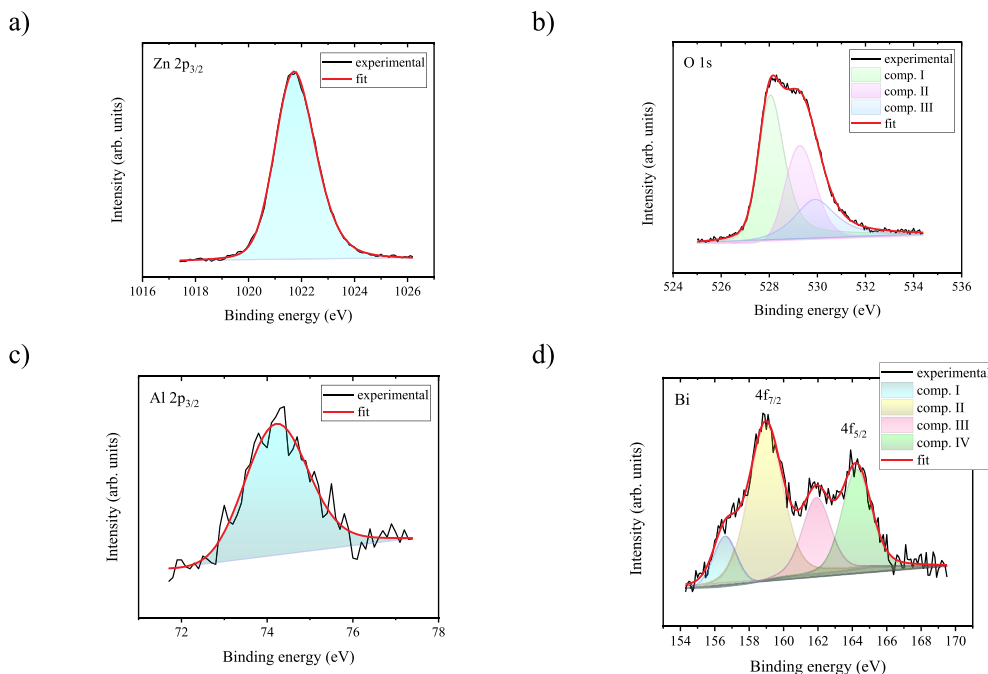


Fig. 4. XPS spectra and respective fits to main photoelectron lines (Zn 2p, O 1s, Al 2p and Bi 4f) for the ZnO:Al,Bi thin film deposited with the highest  $J_{Bi} = 0.26 \text{ mA cm}^{-2}$ , after thermal annealing in vacuum at  $350 \text{ }^\circ\text{C}$ .

### 3.2. ZnO:Ga,Bi films

Fig. 5a) shows the evolution of Bi content in ZnO:Ga,Bi films, measured by different analytical techniques. Blue symbols are ascribed to data from as-deposited (AD) samples, while the red ones refer to samples after a thermal annealing in vacuum at  $350 \text{ }^\circ\text{C}$  (TA). Starting with both EDX and RBS data, again one can observe the same increasing tendency of Bi atomic content with  $J_{Bi}$  for ZnO:Al,Bi films, albeit within a different values range. Between  $0.13 < J_{Bi} < 0.26 \text{ mA cm}^{-2}$  the Bi content increases from 0.1 to 2.4 at.%. The Bi content is thus higher for ZnO:Ga,Bi films when compared with ZnO:Al,Bi films. As for the XPS measurements, the data shows the same exponential tendency but with higher Bi content, varying between 0.7 and 8.8 at.% in the same  $J_{Bi}$  range. Error bars for Bi atomic composition are represented in this figure, being an average of 3% for RBS values and an average of 5% for XPS and EDX findings.

The ionic radii of  $\text{Ga}^{3+}$  and  $\text{Al}^{3+}$  are respectively  $0.47 \text{ \AA}$  and  $0.39 \text{ \AA}$ ; when compared with that of the  $\text{Zn}^{2+}$ ,  $0.60 \text{ \AA}$ , one can assume that the  $\text{Ga}^{3+}$  can easily substitute  $\text{Zn}^{2+}$  in the ZnO wurtzite structure with less lattice distortion than that caused by  $\text{Al}^{3+}$ . Moreover, it is likely that Ga ions only occupy substitutional sites in the ZnO crystal, whereas Al ions occupy both substitutional and interstitial sites. Such lattice

Table 2

Average concentration (at.%) of the elements of the host matrix: ZnO:Ga, calculated from PIXE and RBS measurements.

Element	Zn	O	Ga
Concentration (at.%)	$50.8 \pm 1.4$	$45.4 \pm 2.4$	$2.3 \pm 0.2$

deformations and defects caused by the Al in the ZnO structure are expected to inhibit Bi doping [24]. It is very important to stress that XPS measurements are performed in the first surface layers, between 5 and 7 nm below the film surface, while EDS integrate all layer content without any depth resolution. With RBS it is possible to get an elemental depth profile, although usually with lower surface sensitivity than one obtained with XPS. Thus, the use of different chemical composition characterization techniques may result in a disparity of results due to the intrinsic physical nature of the techniques themselves. The Ga/Zn atomic composition ratio obtained with RBS and XPS is very similar, being between 0.04 and 0.05 for the majority of the ZnO:Ga,Bi films. However, the Bi/Zn atomic composition ratio has a distinct behaviour, as shown in Fig. 5b). From Table 2, Zn content has a small variation ( $50.8 \pm 1.4 \text{ at.}\%$ ) for ZnO:Ga,Bi films with varying  $J_{Bi}$ .

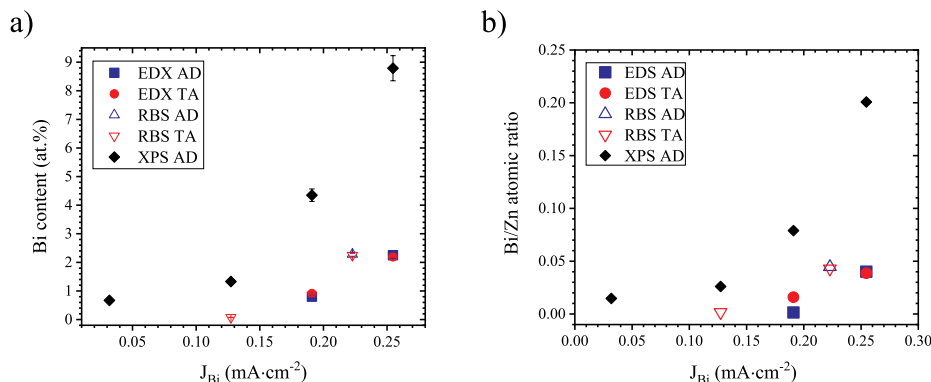


Fig. 5. a) Bi at. % content and b) Bi/Zn atomic composition ratio of ZnO:Ga,Bi thin films as a function of Bi target current density,  $J_{Bi}$ , from EXD, RBS and XPS analyses. Data is represented for as-deposited (AD) and thermal annealed in vacuum at  $350 \text{ }^\circ\text{C}$  (TA) films.

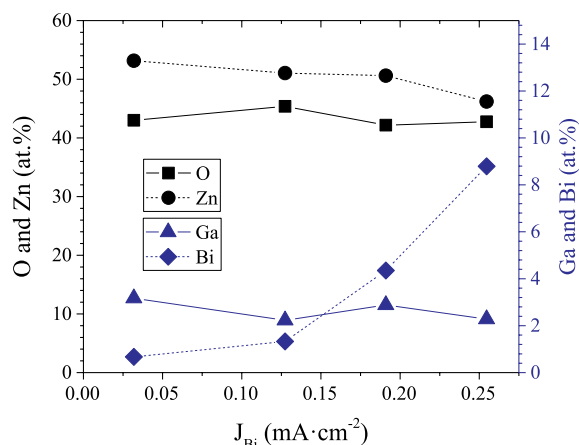


Fig. 6. Elemental composition derived from XPS fits as a function of the Bi target current density of the ZnO:Ga,Bi thin films.

Hence, the discrepancy in results shown in Fig. 5b) suggests Bi segregation to the surface of film deposit. This segregation of Bi in ZnO films has already been reported in the literature [25].

XPS was performed on four as-deposited ZnO:Ga,Bi films with varying  $J_{Bi}$  in order to determine the atomic concentration of the constituent elements; this is presented in Fig. 6. Again, as discussed in the previous section for the RBS results of ZnO:Al,Bi films, oxygen is defective varying in the range of 42–45 at.% (average:  $43.3 \pm 1.2$  at.%). There is a noticeable decrease in Zn content from 53 to 46 at.% (average:  $50.3 \pm 2.5$  at.%) with increasing  $J_{Bi}$ , which is ascribed to the increased incorporation of Bi in the wurtzite structure. Ga average content derived from XPS fits ( $2.6 \pm 0.4$  at.%) matches that obtained from RBS analysis ( $2.3 \pm 0.2$  at.%), within the margin of error, as seen in Table 2. As for the dopant Bi content, with the increase of  $J_{Bi}$  from 0.03 to 0.26 mA cm<sup>-2</sup> it increases concomitantly from 0.7 to 8.8 at.% (as already observed in Fig. 5), which indicates the existence of Bi segregation to the film surface. This is supported by the Bi concentration and Bi/Zn atomic concentration ratio obtained with other techniques, which analyse the whole film thickness and give Bi concentrations and Bi/Zn atomic concentration ratios about 4 times lower.

In order to study the effect of Bi doping into the ZnO wurtzite lattice (hexagonal, *P63mc*) the lattice parameters were determined from Rietveld refinements on the XRD patterns corresponding to ZnO:Ga,Bi films with increasing Bi content (measured from XPS fits). For ZnO:Ga films without Bi the lattice parameters are  $a = 3.190$  Å and  $c = 5.112$  Å. As a comparison, from the ICDD crystallographic card 01-070-8070 the lattice parameters for bulk ZnO are  $a = 3.248$  Å and  $c = 5.205$  Å, with a cell volume of  $47.58$  Å<sup>3</sup>. Hence, the films are in compression residual

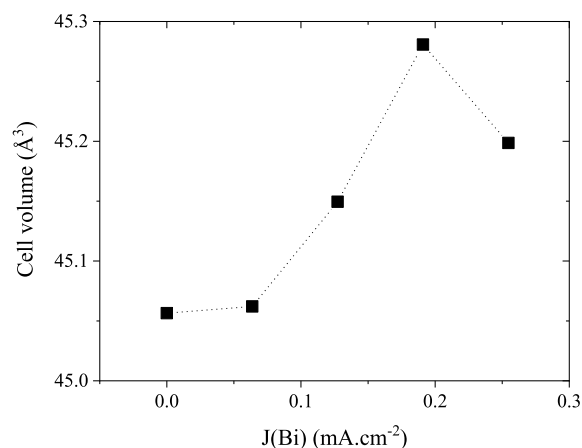
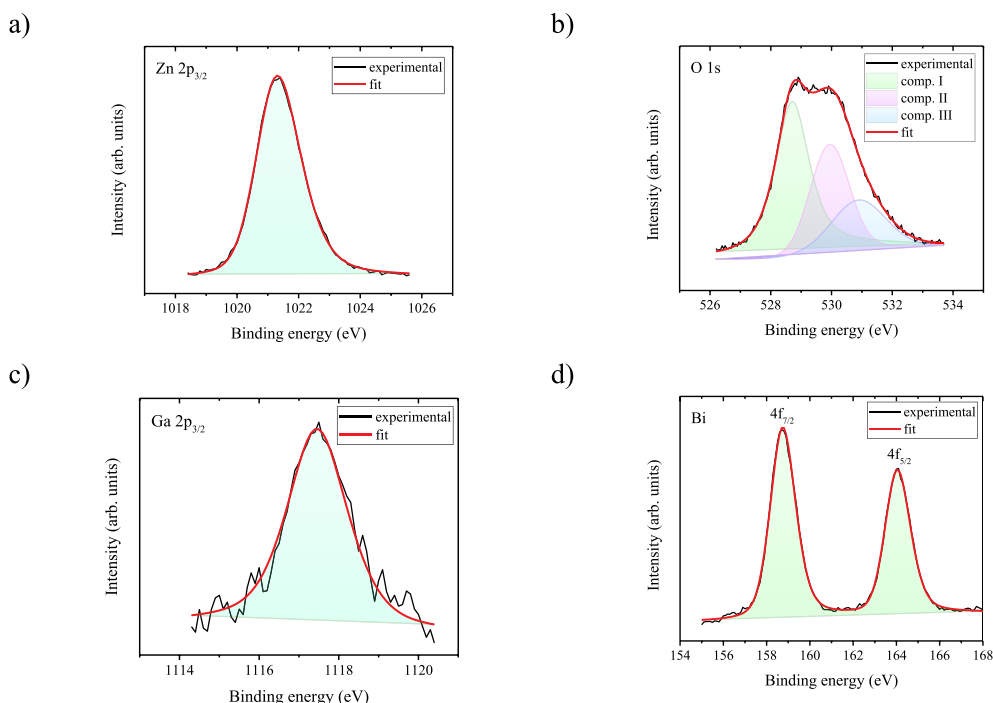


Fig. 7. Variation of the wurtzite unit cell volume with Bi doping for ZnO:Ga,Bi thin films after thermal annealing in vacuum.

stress state, resulting from defects in the microstructure inherent from film growth. From Fig. 7 it can be seen that the wurtzite unit cell volume ( $\frac{\sqrt{3}}{2}a^2c$ ) increases with Bi doping to a maximum of  $45.28$  Å<sup>3</sup> for  $J_{Bi} \approx 0.2$  mA cm<sup>-2</sup>, corresponding to  $\sim 4$  at.% of Bi doping (measured from XPS fits). Above this value the cell volume decreases, possibly due to the aforementioned Bi segregation from the lattice.

In Fig. 8 is displayed the XPS spectra and respective fits to the main photoelectron lines of the as-deposited ZnO:Ga,Bi thin film with highest Bi incorporation (8.8 at.%) corresponding to  $J_{Bi} = 0.26$  mA cm<sup>-2</sup>. Regarding the host cation ( $Zn^{2+}$ ) in the wurtzite cell and the dopant under study ( $Bi^{3+}$ ), both metals are retaining the valency in their known variety of Zn–O and Bi–O polymorphs [23]. From Fig. 8a) the Zn 2p<sub>3/2</sub> core line was fitted with one component (1021.3 eV; FWHM = 1.7 eV), which is ascribed to Zn–O bonds [20]. The binding energy ascribed to the Zn 2p<sub>3/2</sub> core line is 1022 eV and 1021.7 eV for bulk ZnO and Zn metal, respectively [26]. Reports in the literature confirm that for Bi doping in the ZnO wurtzite cell it was possible to resolve a slight decrease in this binding energy (2021.5 eV) when compared to undoped ZnO [23]. Also, it was reported that this Zn 2p<sub>3/2</sub> core line may have some degree of asymmetry when compared to that of bulk ZnO [23]. With this in mind, in Fig. 9 is presented the experimental Zn 2p<sub>3/2</sub> core lines shapes for undoped ZnO (FWHM = 1.8 eV; center: 2022.0 eV; asymmetry:  $-0.02$ ), ZnO:Al,Bi (FWHM = 1.7 eV; center: 2021.7 eV; asymmetry:  $-0.04$ ) and ZnO:Ga,Bi (FWHM = 1.7 eV; center: 2021.3 eV; asymmetry:  $-0.07$ ) films, where it can be perceived a shift to lower binding energies. For both ZnO:Al,Bi and ZnO:Ga,Bi films the corresponding Al and Ga concentration is similar ( $\sim 2$  at.%), while Bi is  $\sim 1$  at.% and  $\sim 9$  at.%, respectively, derived from XPS fits. The registered asymmetry of the Zn 2p<sub>3/2</sub> core lines shapes displayed in Fig. 9, with absolute values given above, was determined from the respective fits using a mixture of Lorentzian/Gaussian functions with a mix ratio of 1:3, with automatic removal of both background [27]. The observed asymmetry in the line shape of the doped films is towards lower binding energies and increases with Bi content, being more prominent in the doped films in respect to undoped ZnO. It can be suggested that Bi doping into the wurtzite lattice increases the asymmetry of the Zn 2p<sub>3/2</sub> core lines. From previous grazing incidence XRD experiments on both ZnO:Al,Bi and ZnO:Ga,Bi films [16] neither Bi<sub>2</sub>O<sub>3</sub> or Bi-metal crystalline phases were discerned in the diffractograms; only diffraction peaks associated with the wurtzite structure, which, with the previous discussion, provides strong evidence Bi is in the wurtzite cell.

Regarding the O 1s core line in Fig. 8b), this was fitted with three components (I, II and III): the main component at 528.7 eV (I) is ascribed with Zn–O bonds; the second component (II) centred at 529.9 eV is associated with defective oxygen (vacancies) and with Bi–O bonds; the third component (III) centred at 530.9 eV is associated with adsorbed oxygen [21,22], as well as with oxygen in Ga<sub>2</sub>O<sub>3</sub> [28]. The relative areas of these three contributions is 50%, 31% and 19%, respectively. Component II of the O 1s photoelectron line, related with oxygen vacancies, has a FWHM of 1.1 eV, which reveals the importance of the defective oxygen sites in the enhancement of the electrical conductivity. In Fig. 8c) the Ga 2p<sub>3/2</sub> core line was fitted with one contribution (1117.5 eV; FWHM = 1.8 eV) related with either Ga–O bonds in the ZnO matrix or with Ga<sub>2</sub>O<sub>3</sub> (which cannot be excluded). Lastly, the Bi 4f core level, shown in Fig. 8d), was fitted into peak doublets with a spin-orbit energy separation of  $4f_{5/2}-4f_{7/2} = 5.3$  eV and a peak ratio  $A_{4f_{5/2}}/A_{4f_{7/2}} = 0.75$ . Two contributions were fitted, with Bi 4f<sub>7/2</sub> binding energies of 156.9 and 158.7 eV, which correspond to the metallic bismuth and oxidation state of  $Bi^{3+}$  in Bi<sub>2</sub>O<sub>3</sub>, respectively [23]. The ratio of this oxide/metal oxidation state varies from 3 to 4 in most of these samples, with the exception of the ZnO:Ga,Bi film that was deposited with the highest value of  $J_{Bi} = 0.26$  mA cm<sup>-2</sup>, where the metal state is absent, as observed in Fig. 8d). Moreover, from Fig. 8d) it can be observed that each of the aforementioned 4f<sub>5/2</sub> and 4f<sub>7/2</sub> doublet peaks have symmetrical line shapes, which is indicative of Bi–O bonds



**Fig. 8.** XPS spectra and respective fits to main photoelectron lines (Zn 2p, O 1s, Ga 2p and Bi 4f) for the as-deposited ZnO:Ga, Bi thin film grown with the highest  $J_{Bi} = 0.26 \text{ mA cm}^{-2}$ .

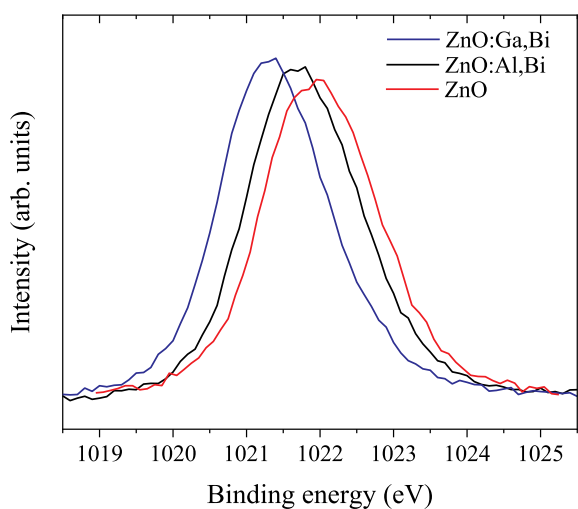


**Fig. 9.** XPS experimental Zn 2p<sub>3/2</sub> core lines shapes for ZnO (FWHM = 1.8 eV; center: 2022.0 eV; asymmetry: -0.02), ZnO:Al,Bi (FWHM = 1.7 eV; center: 2021.7 eV; asymmetry: -0.04; ~2 at% Al, ~1 at% Bi) and ZnO:Ga,Bi (FWHM = 1.7 eV; center: 2021.3 eV; asymmetry: -0.07; ~2 at% Ga, ~9 at% Bi) films.

in the wurtzite cell, since it has been reported in the literature that the XPS core level spectra for Bi metal has asymmetrical line shapes [23]. In a future work Extended X-ray Absorption Fine Structure experiments might enlighten on the coordination of Bi in the ZnO:Ga host matrix.

In Fig. 10 is presented the RBS spectra of a ZnO:Ga,Bi thin film for a sample deposited with  $J_{Bi} = 0.22 \text{ mA cm}^{-2}$  after thermal annealing in vacuum at 350 °C. As for the case of ZnO:Al:Bi films, the Bi signal is clearly visible at high energies, separated from the signals coming from other elements. It changes rapidly, increasing for lower energies. This is proof that the Bi concentration is not constant, instead it increases with depth. From the RBS data, a depth profile can be determined accurately, and the average concentration of Bi can also be determined. Conversely, Ga and Zn have similar masses, and while the total content

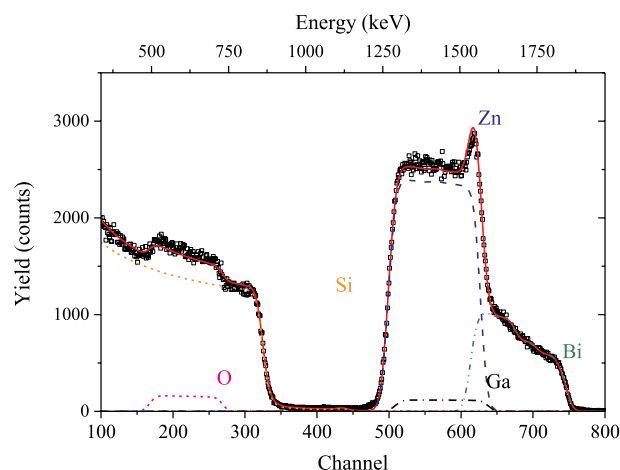


**Fig. 10.** RBS spectra of a ZnO:Ga,Bi thin film deposited with the  $J_{Bi} = 0.22 \text{ mA cm}^{-2}$  after thermal annealing in vacuum at 350 °C.

of Zn and Ga can be easily determined, the accuracy with which their individual concentrations are determined is limited. In this case, the PIXE data, which are extremely sensitive to the total amount of each of those elements, but not to their depth distribution, was used to determine Ga/Zn ratio, as explained below.

From the combined RBS and PIXE fits to all samples, the average composition of the elements from the ZnO:Ga host matrix is given in Table 2; the Bi dopant concentration is given in previously discussed Fig. 5. Hence, all films are oxygen deficient, resulting in films with a high electrical conductivity, as reported elsewhere [16]. In Fig. 11 are displayed two RBS spectra of the same ZnO:Ga,Bi film deposited with a  $J_{Bi} = 0.22 \text{ mA cm}^{-2}$ , taken for the as-deposited and after thermal annealing in vacuum at 350 °C states. From this last figure, it can be observed a Bi surface enrichment for the sample in the as deposited state, which supports the conclusion reached with data presented in Fig. 5. Additionally, and resulting from the thermal annealing, changes in Bi content can be discerned at the surface of the film, since a large portion

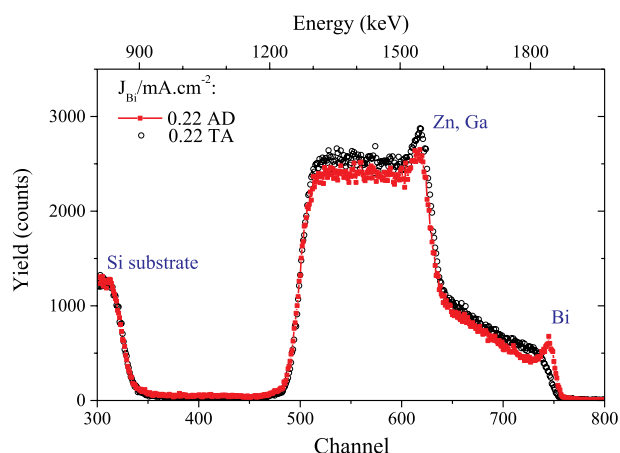


Fig. 11. RBS spectra for a ZnO:Ga,Bi thin films deposited in the same conditions,  $J_{\text{Bi}} = 0.22 \text{ mA cm}^{-2}$ , in the as-deposited (AD) and thermal annealed in vacuum at  $350^\circ\text{C}$  (TA) state.

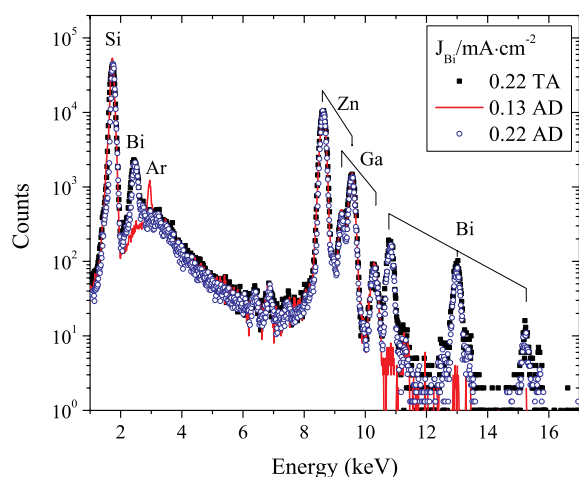


Fig. 12. PIXE spectra from three ZnO:Ga,Bi thin films for the determination of the Ga content. Data is present for as-deposited (AD) and thermal annealed in vacuum at  $350^\circ\text{C}$  (TA) films deposited with varying  $J_{\text{Bi}}$ .

of Bi atoms are depleted from the topmost layers, possibly resulting from thermal evaporation; a similar behaviour was observed in section 3.1 for the ZnO:Al,Bi films. Also from Fig. 11, the Zn content is slightly increased with the thermal annealing in vacuum, but on the expense of oxygen reduction. It has been reported that thermal annealing enhances the origination of oxygen vacancies and subsequent increase in the carrier concentration of certain metal oxide thin films [19,29,30].

From Table 2, combined RBS and PIXE experiments yielded a Ga content in the ZnO:Ga,Bi films of  $2.3 \pm 0.2 \text{ at.}\%$ , which is higher than what is found in the composite ZnO:Ga<sub>2</sub>O<sub>3</sub> sputtering target (1.9 at.%). Since this Ga content in the ZnO:Ga host matrix is also higher than that of Al in the ZnO:Al (1.6 at.%) host matrix, PIXE was used to evaluate Ga atomic concentration in three ZnO:Ga,Bi films deposited and treated in different conditions, as seen in Fig. 12. From this analysis it was estimated the Ga content listed in Table 2, being this value fixed during the RBS fits to the ZnO:Ga,Bi films. A similar analysis could not be performed for the case of ZnO:Al,Bi due to inherent technical difficulties in determining Al content with PIXE, where the signal to noise ratio was very low.

#### 4. Conclusions

A comprehensive study of the composition of ZnO:Al,Bi and ZnO:Ga,Bi films was endured due to the interest in the application of these transparent coating materials for photovoltaic electrodes and

thermoelectric devices. The level of Bi incorporation in the ZnO:Al and ZnO:Ga host matrices was determined by Rutherford backscattering spectrometry coupled with particle-induced X-ray emission experiments, X-ray photoelectron spectroscopy and energy dispersive X-ray spectroscopy. The rationale behind this study regards the optimization of the thermoelectric figure of merit, which is inversely proportional to the thermal conductivity of these films. Since Bi<sup>3+</sup> is a heavier ion with a very large ionic radius (1.03 Å), in comparison to that of Zn<sup>2+</sup> (0.60 Å), it is expected that when the former substitutes the latter in the ZnO wurtzite structure it will hinder phonon vibrations throughout the lattice, hence contributing to the decrease of the thermal conductivity and subsequently enhancing the thermoelectric figure of merit and, indirectly, the thermoelectric power, as reported elsewhere by the authors [16]. From these experiments it was found a correlation between Bi atomic content in the films and the Bi target current density, while these films still remain optically transparent in the visible region; for a  $J_{\text{Bi}}$  above  $0.3 \text{ mA cm}^{-2}$  this optical transmittance is compromised. For the ZnO:Al host matrix a maximum of 1.5 at.% of Bi was registered for  $J_{\text{Bi}} = 0.26 \text{ mA cm}^{-2}$ . The EDX, RBS and XPS data converged well with varying  $J_{\text{Bi}}$ . The average level of Al doping in this host matrix is  $3.4 \pm 0.4 \text{ at.}\%$ , more than twice of the amount found in the host ZnO:Al<sub>2</sub>O<sub>3</sub> target. In the case of the ZnO:Ga host matrix a maximum of 2.4 at.% of Bi was registered for  $J_{\text{Bi}} = 0.26 \text{ mA cm}^{-2}$ , with a surface enrichment content that varied from 1.3 to 8.8 at.% with the increase of  $J_{\text{Bi}}$  from 0.03 to  $0.26 \text{ mA cm}^{-2}$ . It was shown that the wurtzite unit cell volume increases with Bi-doping in the ZnO:Ga,Bi films up to a maximum of  $45.28 \text{ \AA}^3$  for  $J_{\text{Bi}} \approx 0.2 \text{ mA cm}^{-2}$ , decreasing after that; possibly due to Bi segregation from the lattice, as shown from XPS fits. When compared to undoped ZnO, the shift to lower binding energies and asymmetry of the Zn 2p<sub>3/2</sub> core line shapes associated with the ZnO:Al,Bi and ZnO:Ga,Bi films provides evidence of Bi–O bonds in the wurtzite cell, since bismuth oxide or Bi-metal X-ray diffraction peaks are absent in all films. Additionally, from the symmetrical Bi 4f<sub>7/2</sub> and Bi 5/2 core lineshapes further evidence is given to the Bi insertion in the ZnO Wurtzite cell. From RBS experiments, it was found that this surface enrichment of the deposit with Bi atoms is slightly depleted upon post thermal annealing in vacuum at  $350^\circ\text{C}$ . In the latter host matrix, the average Ga composition is  $2.3 \pm 0.2 \text{ at.}\%$ , just slightly above of the value found in the ZnO:Ga<sub>2</sub>O<sub>3</sub> target (1.9 at.%). As previously reported by the authors [16], this level of Al and Ga doping in the respective host matrices is responsible for the increase in charge carrier concentration. Moreover, both ZnO:Al,Bi and ZnO:Ga,Bi films are deficient in oxygen, where the O content is  $44.7 \pm 1.3 \text{ at.}\%$  and  $45.4 \pm 2.4 \text{ at.}\%$ , respectively. This oxygen sub stoichiometry results from oxygen vacancy generation in the wurtzite cell due to the trivalent Al<sup>3+</sup> and Ga<sup>3+</sup> dopant ions, and confirmed from XPS experiments on the O1s photoelectron line. Ongoing experiments with X-ray absorption, Kelvin probe atomic force microscopy and atomic probe tomography will aid to comprehend the inherent mechanisms of Bi incorporation in the ZnO wurtzite lattice, such as its position in the lattice and inherent phonon dispersion effect.

#### Acknowledgements

The authors acknowledge the funding from the following institution Fundação para a Ciência e a Tecnologia (FCT, Portugal)/PIDDAC through the Strategic Funds project reference UID/FIS/04650/2013. Filipe Correia is grateful to the Fundação para a Ciência e a Tecnologia for the Ph.D. Grant SFRH/BD/111720/2015. Paulo Salvador is grateful to the Project WinPSC - POCI-01-0247-FEDER-017796, for the research grant, co-funded by the European Regional Development Fund (ERDF), through the Operational Programme for Competitiveness and Internationalisation (COMPETE 2020), under the PORTUGAL 2020 Partnership Agreement. Joana Ribeiro is grateful to University of Minho for the Grant UMINHO/BI/66/2017.

## References

- [1] A. Janotti, C.G. Van de Walle, Fundamentals of zinc oxide as a semiconductor, *Rep. Prog. Phys.* 72 (2009) 126501, <https://doi.org/10.1088/0034-4885/72/12/126501>.
- [2] Ü. Özgür, Y.I. Alivov, C. Liu, A. Teke, M.A. Reshchikov, S. Doğan, V. Avrutin, S.J. Cho, H. Morkoç, A comprehensive review of ZnO materials and devices, *J. Appl. Phys.* 98 (2005) 1–103, <https://doi.org/10.1063/1.1992666>.
- [3] T. Tynell, M. Karppinen, Atomic layer deposition of ZnO: a review, *Semicond. Sci. Technol.* 29 (2014), <https://doi.org/10.1088/0268-1242/29/4/043001>.
- [4] K. Ellmer, A. Bikowski, Intrinsic and extrinsic doping of ZnO and ZnO alloys, *J. Phys. D Appl. Phys.* 49 (2016), <https://doi.org/10.1088/0022-3727/49/41/413002>.
- [5] H. Chen, Y. Liu, C. Xie, J. Wu, D. Zeng, Y. Liao, A comparative study on UV light activated porous TiO<sub>2</sub> and ZnO film sensors for gas sensing at room temperature, *Ceram. Int.* 38 (2012) 503–509, <https://doi.org/10.1016/j.ceramint.2011.07.035>.
- [6] M. Al-Fandi, R. Oweis, B.A. Albiss, T. Alzoubi, M.A. Al-Akhras, H. Qutaish, H. Khwailah, S. Al-Hattami, E. Al-Shawwa, A prototype ultraviolet light sensor based on ZnO nanoparticles/graphene oxide nanocomposite using low temperature hydrothermal method, *IOP Conf. Ser. Mater. Sci. Eng.* 92 (2015), <https://doi.org/10.1088/1757-899X/92/1/012009>.
- [7] K.C. Lai, C.C. Liu, C. Hsiung Lu, C.H. Yeh, M.P. Hwang, Characterization of ZnO:Ga transparent contact electrodes for microcrystalline silicon thin film solar cells, *Sol. Energy Mater. Sol. Cells* 94 (2010) 397–401, <https://doi.org/10.1016/j.solmat.2009.12.002>.
- [8] C.G. Granqvist, Transparent conductors as solar energy materials: a panoramic review, *Sol. Energy Mater. Sol. Cells* 91 (2007) 1529–1598, <https://doi.org/10.1016/j.solmat.2007.04.031>.
- [9] T.J. Coutts, D.L. Young, X. Li, Characterization of transparent conducting oxides, *MRS Bull.* (2011), <https://doi.org/10.1557/mrs2000.152>.
- [10] B.A. Albiss, W.A. Sakhaneh, I. Jumah, I.M. Obaidat, NO<sub>2</sub> gas sensing properties of ZnO/Single-Wall carbon nanotube composites, *IEEE Sensor. J.* 10 (2010) 1807–1812, <https://doi.org/10.1109/JSEN.2010.2049739>.
- [11] T. Yamada, A. Miyake, S. Kishimoto, H. Makino, N. Yamamoto, T. Yamamoto, Low resistivity Ga-doped ZnO thin films of less than 100 nm thickness prepared by ion plating with direct current arc discharge, *Appl. Phys. Lett.* 91 (2007) 1–4, <https://doi.org/10.1063/1.2767213>.
- [12] F. Wu, L. Fang, Y.J. Pan, K. Zhou, L.P. Peng, Q.L. Huang, C.Y. Kong, Seebeck and magnetoresistive effects of Ga-doped ZnO thin films prepared by RF magnetron sputtering, *Appl. Surf. Sci.* 255 (2009) 8855–8859, <https://doi.org/10.1016/j.apsusc.2009.06.076>.
- [13] J.N. Duenow, T.A. Gessert, D.M. Wood, B. Egaas, R. Noufi, T.J. Coutts, Investigation of ZnO:Al doping level and deposition temperature effects on CIGS solar cell performance, *MRS Proc* 1012 (2007).
- [14] N. Vogel-Schäuble, Y.E. Romanyuk, S. Yoon, K.J. Saji, S. Populoh, S. Pokrant, M.H. Aguirre, A. Weidenkaff, Thermoelectric properties of nanostructured Al-substituted ZnO thin films, *Thin Solid Films* 520 (2012) 6869–6875, <https://doi.org/10.1016/j.tsf.2012.07.046>.
- [15] P. Mele, S. Saini, H. Honda, K. Matsumoto, K. Miyazaki, H. Hagino, A. Ichinose, Effect of substrate on thermoelectric properties of Al-doped ZnO thin films, *Appl. Phys. Lett.* 102 (2013) 253903, <https://doi.org/10.1063/1.4812401>.
- [16] F.C.C. Correia, P.B.B. Salvador, J.M.M. Ribeiro, A. Mendes, C.J.J. Tavares, Effect on the electrical and morphological properties of Bi incorporation into ZnO:Ga and ZnO:Al thin films deposited by confocal magnetron sputtering, *Vacuum* 152 (2018) 252–260, <https://doi.org/10.1016/j.vacuum.2018.03.033>.
- [17] N.P. Barradas, C. Jeaynes, R.P. Webb, U. Kreissig, R. Grötzschel, Unambiguous automatic evaluation of multiple ion beam analysis data with simulated annealing, *Nucl. Instrum. Methods Phys. Res. Sect. B Beam Interact. Mater. Atoms* 149 (1999) 233–237, [https://doi.org/10.1016/S0168-583X\(98\)00731-9](https://doi.org/10.1016/S0168-583X(98)00731-9).
- [18] M. Chen, X. Wang, Y. Yu, Z. Pei, X. Bai, C. Sun, R. Huang, L. Wen, X-ray photoelectron spectroscopy and auger electron spectroscopy studies of Al-doped ZnO films, *Appl. Surf. Sci.* 158 (2000) 134–140, [https://doi.org/10.1016/S0169-4332\(99\)00601-7](https://doi.org/10.1016/S0169-4332(99)00601-7).
- [19] M.V. Castro, L. Rebouta, P. Alpuim, M.F. Cerqueira, M. Benelmekki, C.B. Garcia, E. Alves, N.P. Barradas, E. Xuriguera, C.J. Tavares, Optimisation of surface treatments of TiO<sub>2</sub>: Nb transparent conductive coatings by a post-hot-wire annealing in a reducing H<sub>2</sub> atmosphere, *Thin Solid Films* 550 (2014) 404–412, <https://doi.org/10.1016/j.tsf.2013.11.044>.
- [20] G. Schon, Elsevier Scientific Publishing, *J. Electron Spectros. Relat. Phenomena* 2 (1973) 75–86, [https://doi.org/10.1016/0006-8993\(75\)90185-7](https://doi.org/10.1016/0006-8993(75)90185-7).
- [21] F. Wu, L. Fang, Y.J. Pan, K. Zhou, Q.L. Huang, C.Y. Kong, Effect of substrate temperature on the structural, electrical and optical properties of ZnO:Ga thin films prepared by RF magnetron sputtering, *Phys. E Low-Dimensional Syst. Nanostructures* 43 (2010) 228–234, <https://doi.org/10.1016/j.physe.2010.07.007>.
- [22] M.C. Biesinger, B.P. Payne, A.P. Grosvenor, L.W.M. Lau, A.R. Gerson, R.S.C. Smart, Resolving surface chemical states in XPS analysis of first row transition metals, oxides and hydroxides: Cr, Mn, Fe, Co and Ni, *Appl. Surf. Sci.* 257 (2011) 2717–2730, <https://doi.org/10.1016/j.apsusc.2010.10.051>.
- [23] D.A. Zatsepin, D.W. Boukhvalov, N.V. Gavrilov, E.Z. Kurmaev, I.S. Zhidkov, XPS and DFT study of pulsed Bi-implantation of bulk and thin-films of ZnO—the role of oxygen imperfections, *Appl. Surf. Sci.* 387 (2016) 1093–1099, <https://doi.org/10.1016/j.apsusc.2016.07.045>.
- [24] C.Y. Tsay, W.T. Hsu, Comparative studies on ultraviolet-light-derived photo-response properties of ZnO, AZO, and GZO transparent semiconductor thin films, *Materials* 10 (2017) 1–13, <https://doi.org/10.3390/ma10121379>.
- [25] J.W. Lee, N.G. Subramaniam, J.C. Lee, S. Kumar, T.W. Kang, Study of stable p-type conductivity in bismuth-doped ZnO films grown by pulsed-laser deposition, *Epl* 95 (2011), <https://doi.org/10.1209/0295-5075/95/47002>.
- [26] Thermo Scientific XPS, XPS Ref. Table Elem, (2018) <https://xpssimplified.com/elements/zinc.php>, Accessed date: 21 December 2018.
- [27] I. Kojima, M. Kurahashi, Application of asymmetrical Gaussian/Lorentzian mixed function for X-ray photoelectron curve synthesis, *J. Electron. Spectrosc. Relat. Phenom.* 42 (1987) 177–181, [https://doi.org/10.1016/0368-2048\(87\)85018-1](https://doi.org/10.1016/0368-2048(87)85018-1).
- [28] S.C. Ghosh, M.C. Biesinger, R.R. Lapierre, P. Kruse, X-ray photoelectron spectroscopic study of the formation of catalytic gold nanoparticles on ultraviolet-ozone oxidized GaAs(100) substrates, *J. Appl. Phys.* 101 (2007) 114322, <https://doi.org/10.1063/1.2743729>.
- [29] M.V. Castro, M.F. Cerqueira, L. Rebouta, P. Alpuim, C.B. Garcia, G.L. Júnior, C.J. Tavares, Influence of hydrogen plasma thermal treatment on the properties of ZnO:Al thin films prepared by dc magnetron sputtering, *Vacuum* 107 (2014) 145–154, <https://doi.org/10.1016/j.vacuum.2014.04.022>.
- [30] M.V. Castro, C.J. Tavares, Dependence of Ga-doped ZnO thin film properties on different sputtering process parameters: substrate temperature, sputtering pressure and bias voltage, *Thin Solid Films* 586 (2015) 13–21, <https://doi.org/10.1016/j.tsf.2015.04.036>.